ACS OMEGA

http://pubs.acs.org/journal/acsodf

Article

Enhanced Oral Vaccine Efficacy of Polysaccharide-Coated Calcium Phosphate Nanoparticles

Pei Cao, Felicity Y. Han, Lisbeth Grøndahl, Zhi Ping Xu,* and Li Li*

Cite This: *ACS Omega* 2020, 5, 18185−18197

Read Online

ACCESS | Metrics & More | Article Recommendations | Supporting Information

ABSTRACT: Oral administration of vaccines has been limited due to low immune response compared to parenteral administration. Antigen degradation in the acidic gastrointestinal environment (GI), mucus barriers, and inefficient cellular uptake by immune cells are the major challenges for oral vaccine delivery. To solve these issues, the current study investigates calcium phosphate nanoparticles (CaP NPs) coated with polysaccharides as nanocarriers for oral protein antigen delivery. In this design, the CaP NP core had an optimized antigen encapsulation capacity of 90 mg (BSA-FITC)/g (CaP NPs). The polysaccharides chitosan and alginate were coated onto the CaP NPs to protect the antigens against acidic degradation in the GI environment and enhance the immune response in the small intestine. The antigen release profiles showed that alginate-chitosan-coated CaP NPs prevented antigen release in a simulated gastric fluid (pH 1.2), followed by sustained release in simulated intestinal (pH 6.8) and colonic (pH 7.4) fluids. Cellular uptake and macrophage stimulation data revealed that the chitosan coating enhanced antigen uptake by intestine epithelia cells (Caco-2) and macrophages and improved surface expression of costimulatory molecules on macrophages. *In vivo* test further demonstrated that oral administration of alginate-chitosan-coated CaP@OVA NPs significantly enhanced the mucosal IgA and serum IgG antibody responses as compared to naked OVA, indicating that the CaP-Chi-Alg nanoparticle can potentially be used as a promising oral vaccine delivery system.

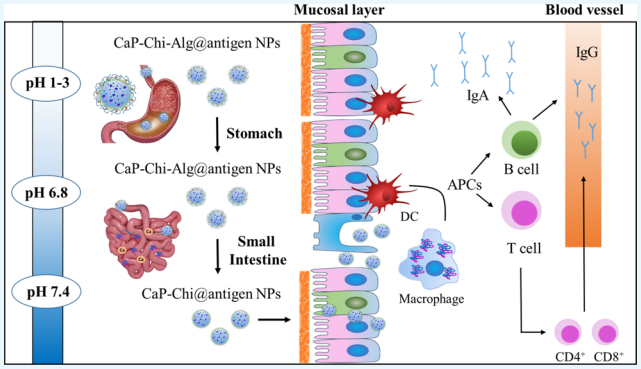

INTRODUCTION

Vaccination has been broadly used worldwide and plays a key role in preventing outbreak of infectious diseases for humans and animals.[1] Recently, peptides and proteins have been developed and used as antigens against infectious diseases due to their excellent selectivity and efficiency.[2−4] They are mainly administered parenterally (intramuscularly or subcutaneously), but the injected vaccines are often associated with intensive handling, low patient compliance, and cross-infections induced by the contamination of needles at the injection site.[3,5,6] Oral administration of the protein or peptide vaccine is an attractive alternative route for vaccine delivery to produce both systemic and mucosal immune responses.[7] Its convenience, minimal pain, simplicity, and non-invasive nature further improve the patient compliance and reduce side effects and cross-infections.[8] Currently, several oral vaccines that target pathogens such as poliovirus, cholera, and salmonella have been licensed to human and animal use globally.[9] However, the oral vaccination efficiency is relatively poor and inconsistent compared to that of the injected administration due to degradation of the antigen in the acidic gastrointestinal tract (GI) environment, uncontrolled release of antigens, the low mucosal permeability, and cellular uptake in the intestine.[10]

Nanoparticles (NPs) of different compositions based on liposomes, micelles, polymers, and inorganic materials have been developed as vaccine carriers to deliver antigens.[11] For example, calcium phosphate (CaP) has been considered as a promising adjuvant for vaccine delivery due to its high antigen loading capacity, excellent biodegradation, and low cytotoxicity as well as the simple preparation method.[12−14] Compared to alumina gel and bacteria toxins, CaP has shown enhanced IgG1 production and reduced IgE antibody response after the administration of tetanus, diphtheria, or pertussis toxoid antigens in mice.[15] Temchura et al. developed CaP NPs with an average particle size of 200 nm as a carrier and adjuvant for vaccine delivery and effectively increased surface expression of B-cell activation markers.[16] It has been reported that particle size, charge, and surface properties of NPs have significant effects on the antigen adsorption and penetration in the

Received: April 18, 2020
Accepted: July 6, 2020
Published: July 17, 2020

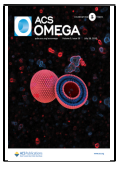

https://dx.doi.org/10.1021/acsomega.0c01792
ACS Omega 2020, 5, 18185−18197

intestine.[17] When the size of the particles is larger than the pore size of the mucus (100−500 nm), the particles can be excluded from the mucus layer.[18] Recently, in our group, lipid-coated CaP NPs with a size of 20−40 nm have been developed for drug and gene delivery and have shown significantly enhanced treatment efficacy when delivered to tumors.[19,20] Thus, using CaP NPs as carriers for vaccine delivery could potentially improve cellular uptake of antigens by antigen-presenting cells (APCs) such as macrophages and dendritic cells to enhance the immune response. Although CaP NP delivery systems are well established for the delivery of antigens as carriers and adjuvants by subcutaneous injection, only a few have been developed for oral vaccine delivery due to their poor stability in the acidic GI environment.[14,21]

To further improve mucosal vaccine delivery efficiency, several mucosal penetrating polymers including chitosan and pectin have been used to coat the surface of NPs. These mucosal penetrating polymers have shown strong mucus attachment, prolonged the residence time at the mucosal surface, and improved mucus penetration.[22−24] For example, a chitosan- and alginate-coated LDH NP system was developed for oral vaccine delivery.[25] The chitosan-coated LDH NPs strongly adsorbed BSA or OVA and efficiently enhanced the cellular uptake of BSA or OVA in intestine epithelial cells and macrophages. In addition, alginate has been widely used for oral drug/vaccine delivery to protect bioactive compounds against the acidic/enzymatic degradation at the harsh GI environment.[26,27] Huma et al. reported that lactoferrin (Lf)-loaded alginate microgel particles can efficiently provide protection from the action of pepsin in the SGF and allow Lf release in the SIF.[28] Considering the opposite charges of chitosan and alginate, these polymers form polyelectrolyte complexes facilitating the formation of coatings.[29,30]

In this work, we have rationally designed chitosan- and alginate-coated CaP NPs (CaP-Chi-Alg NPs) with a particle size smaller than 50 nm as antigen carriers for oral vaccine delivery. The encapsulation efficiency and capacity of proteins (BSA or OVA) were optimized by varying the ratios of Ca to P and protein concentration during the NP fabrication. The antigen-CaP NPs were coated with chitosan and alginate in a step-wise manner. Through *in vitro*-simulated environments, we have evaluated the antigen release in the acidic GI environment followed by antigen release at pH 6.8 and 7.4. Cellular uptake was evaluated *in vitro* in intestine epithelial cells (Caco-2) and macrophages (RAW264.7). The immune IgA and IgG responses of OVA-encapsulated CaP-Chi-Alg NPs were evaluated in a mouse model and *in vivo* studies exhibited that OVA-encapsulated CaP-Chi-Alg NPs enhanced specific immune response compared to free OVA. Overall, our findings show that the CaP-Chi-Alg NPs developed in this research have a potential as an oral vaccine delivery vehicle.

MATERIALS AND METHODS

Materials. Chitosan (medium molecular weight (50−190 kDa); degree of deacetylation of 75−85%), IGEPAL CO-520, sodium chloride, calcium chloride dihydrate, bovine serum albumin-FITC (BSA-FITC), albumin from white chicken egg (OVA; purity, ≥98%), glycerol, and goat anti-mouse IgG-HRP were all purchased from Sigma. Sodium alginate was purchased from the Melbourne Food Depot and cyclohexane was obtained from Ajax Finechem. Disodium hydrogen orthophosphate was from AnalaR. Soybean trypsin inhibitor was purchased from FUJIFILM Chemical. TMB single solution was bought from Life Technologies and goat anti-mouse IgA, IgG2a, and IgG1-HRP were all purchased from Southern Biotech. Trypsin−EDTA (0.25%), PBS buffer (37 mmol/L NaCl, 2.7 mmol/L KCl, 8.1 mmol/L Na_2HPO_4, and 1.47 mmol/L KH_2PO_4; pH 7.4) and DMEM medium were obtained from Life Technologies Corporation (Australia).

Preparation of CaP and CaP@BSA-FITC NPs. The CaP nanoparticles (CaP NPs) were prepared by a modified reverse microemulsion method based on our previous report.[20] In brief, a W/O microemulsion containing $CaCl_2$ was prepared by mixing 150 μL of 5.0 M $CaCl_2$ with 5 mL of mixed cyclohexane/Igepal CO-520 (7/3, v/v). A similar microemulsion containing Na_2HPO_4 was prepared by mixing 150 μL of Na_2HPO_4 (pH 9.0) with 5 mL of mixed cyclohexane/Igepal CO-520 (7/3, v/v). Then, the Na_2HPO_4 microemulsion was added into the $CaCl_2$ microemulsion and continuously stirred for 20 min at room temperature. The Ca/P molar ratio was controlled in the range from 1 to 150. The synthesized CaP NPs were collected by adding 10 mL of absolute ethanol and centrifuging at 15000*g* for 20 min at 15 °C and washed three times with ethanol and then twice with water.

BSA-FITC was selected as a model protein and used to determine the protein loading efficiency and capacity as well as cellular uptake. The fabrication of protein-loaded CaP NPs was similar to the CaP NP preparation. First, a BSA-FITC solution (2.0−50.0 mg/mL, 15 μL) was mixed with each of the W/O microemulsions containing 150 μL $CaCl_2$ solution or 150 μL Na_2HPO_4 solution. The Na_2HPO_4 microemulsion with BSA-FITC was added and mixed with the $CaCl_2$ microemulsion with BSA-FITC or BSA under stirring for 20 min. The NP isolation process was the same as described for the CaP NPs.

Protein Encapsulation Efficiency and Capacity. The encapsulation efficiency and capacity of BSA-FITC in the CaP NPs were determined using the approach reported by our group.[20] First, a certain amount of CaP@BSA-FITC NPs was dissolved in the lysis buffer (2 mM EDTA, 0.05% Triton X-100, 0.1 M Tris buffer, pH 7.8) at 65 °C for 10 min to release the entrapped BSA-FITC. The amount of BSA-FITC in the CaP NPs measured at 525 nm using a plate reader against a BSA-FITC standard curve in lysis buffer. The encapsulation efficiency (EE%) and capacity (EC, mg/g) of BSA-FITC in the CaP NPs were calculated based on the following equations:

$$\mathrm{EE\%} = (w_t/w_o) \times 100\%$$

$$\mathrm{EC} = w_t/w_{\mathrm{CaP}}$$

where w_t is the amount of the BSA-FITC (mg) encapsulated in CaP, w_{CaP} is the total weight of calcium phosphate nanoparticle (g), and w_0 is the total amount of BSA-FITC (mg) added in the microemulsion.

Preparation of Polymer-Coated CaP@BSA-FITC NPs. The chitosan-coated CaP NPs (CaP-Chi@BSA-FITC) and chitosan/alginate-coated CaP (CaP-Chi-Alg@BSA-FITC) were prepared via a layer-by-layer approach. The prepared CaP@BSA-FITC (Ca/P ratio of 50) in the emulsion (10 mL, pH ≈ 7) were mixed with 100 μL of chitosan (0.5%) and continuously stirred for 20 min, followed by centrifugation and ethanol and water wash as described above for the NP isolation process. Then, the collected CaP-Chi@BSA-FITC NPs were dispersed in distilled water (2 mL) and mixed with 100 μL of alginate solution (0.5%). The resulting suspension was stirred for 20 min, isolated by centrifuging at 15000*g* for 20 min, and washed three times with water to prepare the CaP-Chi-Alg@

https://dx.doi.org/10.1021/acsomega.0c01792
ACS Omega 2020, 5, 18185−18197

BSA-FITC NPs. CaP-Alg@BSA-FITC NPs were synthesized with the same procedure as CaP-Chi@ BSA-FITC NPs. For NP systems with different chitosan-to-alginate ratios, the chitosan coating process was kept constant and as described above, while the alginate concentration was adjusted according to the intended ratio.

Physicochemical Characterization. The hydrodynamic diameter and zeta potential were measured by dynamic light scattering (DLS) using a Malvern Nanosizer at 25 °C. According to the literature, the zeta potential of nanoparticles is affected by the buffers during DLS measurement.[31−33] Therefore, all samples were dispersed in DI water for DLS measurement. All data were obtained by measuring a suspension in triplicate and the average value was calculated. The morphology and size distribution of the NPs were characterized using a HITACHI 7700A electron microscope with an acceleration voltage of 80 kV. A total of 100 NPs were measured to generate the size distribution. Protein negative staining was done by applying 5 uL of 0.5% uranyl acetate onto the TEM grid, leaving it for 3−5 min, then drawing off excess from the edge of the grid with filter paper, and the samples were characterized with electron microscopy. Fourier transform infrared (FT-IR) spectroscopy of the NPs was collected on Nicolet 6700 with 2 cm^{-1} resolution and 32 scans in the range between 4000 and 400 cm^{-1}. The CaP and CaP-based NPs were characterized using X-ray diffraction (XRD, Rigaku Miniflex X-ray diffractometer) with a scanning rate at 2°/min in the 2θ range from 5° to 80° using Cu Kα radiation (λ = 0.15406 nm). ICDD 9−432 and JCPDS 090169 were used to identify the crystal phases of NPs.

***In Vitro* Release of BSA-FITC.** The *in vitro* release profiles of BSA-FITC from various NP systems were investigated in simulated gastrointestinal solutions at pH 1.2 (HCl solution), 6.8 (1× PBS buffer, 0.1 M HCl to adjust pH), and 7.4 (1× PBS buffer) for a total time of 8 h. The pH values were chosen to mimic the physiological conditions of SCF (pH 7.4), SIF (pH 6.8), and SGF (pH 1.2). First, a given amount of NPs (5.0 mg) was mixed with 10 mL of SGF under constant stirring and kept in a thermostatic bath at 37 °C. After 2 h, the samples were centrifuged at 15000 rpm for 15 min, the NPs were dispersed in the SIF (pH 6.8) and stirred for 2 h, then the pH was adjusted to 7.4 via NaOH to mimic the SCF, and the mixture was incubated for 4 h. To monitor the release process, an aliquot of the supernatant (0.5 mL) was taken at certain time points and replaced with the same volume of fresh buffer. The concentration of BSA-FITC released from the NPs was determined using a plate reader at 525 nm against a BSA-FITC standard curve in the respective buffer.

Sodium dodecyl sulfate−polyacrylamide gel electrophoresis (SDS-PAGE) was used to determine the BSA-FITC release in the three buffers described above. Briefly, 5 mg of CaP-Chi@ BSA-FITC or CaP-Chi-Alg@BSA-FITC NPs was mixed with SCF, SIF, or SGF solution. The samples were incubated in a 37 °C shaking water bath. At each predetermined time point, the medium (0.5 mL) was withdrawn and 10 μL of the medium was added in the lanes of SDS-PAGE. Free BSA-FITC (4 μg in 10 μL) was added in lane 1 as the reference. Electrophoresis was carried out at a voltage of 100 V for 30 min. The image of the agarose gel was recorded using a Geldoc (Bio-Rad Laboratories, Inc., Hercules, CA).

***In Vitro* Cellular Uptake and Cytotoxicity.** The cellular uptake of BSA-FITC was investigated in the human epithelial colorectal cell line (Caco-2) and the mouse macrophage cell line (RAW 264.7) using confocal microscopy and flow cytometry. Caco-2 and RAW264.7 cells were cultured in DMEM medium (containing 10% fetal bovine serum, 100 U/mL penicillin, and 100 μg/mL streptomycin) at 37 °C in the humidified atmosphere with 5% CO_2. Caco-2 cells were seeded in 12-well plates at a cell density of 1.0×10^5 cells per well and incubated in DMEM medium. After incubation overnight, the cells were treated with fresh DMEM medium containing NPs incubated at 37 °C for 1, 4, 8, or 24 h at BSA-FITC concentrations of 1.0 μg/mL or 0.5, 1.0, 2.0, 4.0, and 8.0 μg/mL for 8 h. After washing three times with PBS (pH 7.4), the cells were fixed using 2% paraformaldehyde/PBS at room temperature and subsequently analyzed by flow cytometry (Accuri C6 flow cytometer, BD Biosciences). The mean fluorescence intensity (MFI, λ = 525 nm) was used to represent the cellular uptake efficiency of BSA-FITC. A similar process was applied to macrophage cells, which were cultured at 37 °C for 0.5, 1, 2, 4, or 8 h at the BSA-FITC concentration of 1.0 μg/mL or at 0.25, 0.5, 1.0, 2.0, and 4.0 μg/mL for 4 h.

For confocal microscopy imaging, Caco-2 and RAW 264.7 cells were seeded on the coverslips in a 24-well plate at a density of 5×10^4 cells per well for 24 h in DMEM medium with 10% FBS and penicillin (10 U/mL)/streptomycin (10 μg/mL) at 37 °C with 5% CO_2. Then, 1 mL of culture medium with NPs at the BSA-FITC concentration of 1 μg/mL was added into the plate and the cells were incubated for 4 or 8 h. Then, the cells were washed three times with PBS, fixed with 4% paraformaldehyde (PFA), and moved to the glass slide containing 4,6-diamidino-2phenylindole (DAPI). After staining for 5 min, the cells on the coverslip were imaged in a Leica SP8 confocal laser scanning microscope.

The cytotoxicity of the NPs was evaluated by 3-(4,5-dimethylthiazol-2-yl)-2,5-diphenyltetrazolium bromide (MTT) assay. Caco-2 and RAW 264.7 cells were seeded in 96-well plates with 5×10^3 cells per well in 200 μL of DMEM medium for 24 h to allow cell attachment. Then, the cells were treated in fresh DMEM medium containing CaP NPs in the concentrations range of 5−400 μg/mL for 48 h. Then, 50 μL of 5.0 mg/mL MTT was added to each well and the plates were incubated for 4 h in a dark room. After removing the MTT-containing DMEM medium, 250 μL of DMSO was added to each well to dissolve the MTT formazan. The absorbance of the converted dye was measured at 490 and 565 nm using the plate reader. The cell viability was calculated using the following equation:

$$\text{cell viability}(\%) = (A_s/A_{\text{control}}) \times 100\%$$

where A_s is the absorbance of cells treated under various conditions, and A_{control} is the absorbance of the cells in the standard medium.

Cell Surface Marker Expression Analysis by Flow Cytometry. In this study, ovalbumin (OVA) was used as the model antigen to test the immune response. CaP@OVA and CaP-Chi@OVA were prepared using the similar process of CaP@BSA-FITC with or without polymer coating. RAW 264.7 cells were seeded in 12-well plates at a cell density of 1×10^5 cells/well for 24 h at 37 °C with 5% CO_2. Then, the cells were treated with a fresh DMEM medium containing CaP@OVA, CaP-Chi@OVA, or free OVA at the OVA concentration of 15.0 μg/mL. Untreated and lipopolysaccharide (LPS)-stimulated macrophage cells (LPS, 50.0 ng/mL) were used as negative and positive controls, respectively. After 24 h incubation, cells were washed three times with PBS buffer

https://dx.doi.org/10.1021/acsomega.0c01792
ACS Omega 2020, 5, 18185−18197

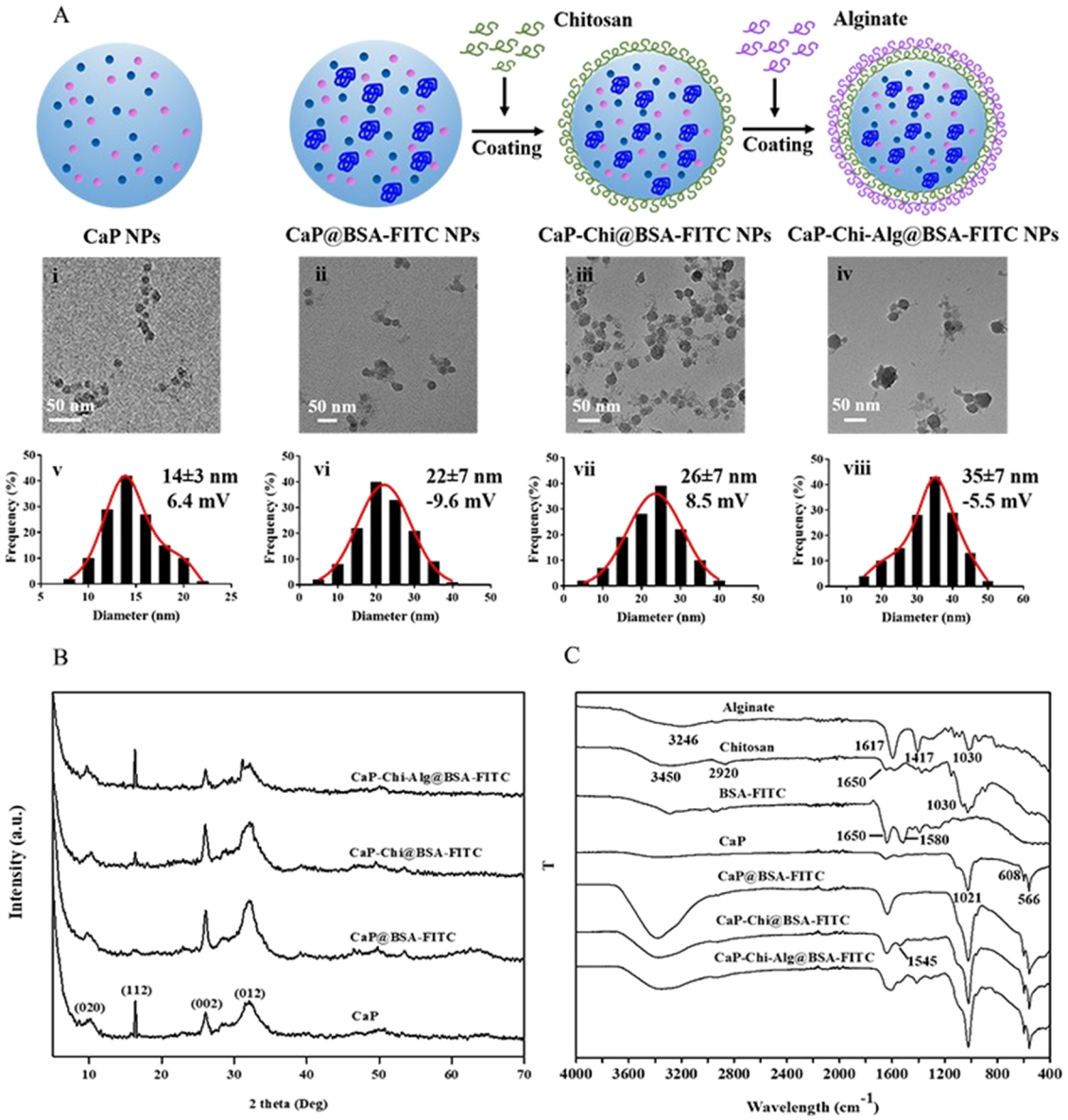

Figure 1. (A) Schematic diagram of the synthetic process and proposed structures of CaP-Chi-Alg@BSA-FITC NPs; (i−iv) TEM images of CaP, CaP@BSA-FITC, CaP-Chi@BSA-FITC, and CaP-Chi-Alg@BSA-FITC; (v−viii) particle size distribution (n = 100) and zeta potential of CaP, CaP@BSA-FITC, CaP-Chi@BSA-FITC, and CaP-Chi-Alg@BSA-FITC. (B) XRD pattern and (C) FTIR spectra of CaP-based NPs.

containing 2% BSA at pH 7.4. Cells were then stained with antibodies that bind to mouse CD80, CD86, CD40, and I-E/I-A (MHC-II) (BioLegend) for 30 min at 4 °C. After washing three times with 1× PBS solution with 2% BSA (pH ≈ 7.4), cells were fixed in 4% PFA and analyzed on an Accuri C6 flow cytometer.

Animals and Immunizations. Animal experiments were performed in accordance with approval from the University of Queensland Animal Ethics Committee, Australia (AIBN/224/18). Female C57BL/6J (6−8 weeks) mice were purchased from University of Queensland Biological Resources. Mice were housed in cages with free access to standard diet and acclimated a week prior to treatment. On day 0, mice were randomly divided into three groups and treated with CaP-Chi-Alg@OVA NPs, OVA solution, and PBS (control group) (n = 6). A dose or equivalent dose of OVA (200 μg) was administrated by oral gavage on days 0, 2, and 4 and boosted on day 14 and 21. Mice were anesthetized with 5% isoflurane in 100% oxygen and then maintained using 1−2% isoflurane in 100% oxygen. Blood samples were collected via the tail tip at day 0, 14, and 35 before dosing, then placed at room temperature for 30 min, and centrifuged at 4 °C for 20 min at 1000g. The sera were collected and stored at −80 °C. The mice were euthanized using CO_2 inhalation at day 35.

To determine mucosal IgA antibody responses, fecal pellets (FPs) were collected from each mouse at days 0 and 14 and weighted. FPs were emulsified in 1 mL of 1 × PBS containing 0.1 mg/mL of soybean trypsin inhibitor (STI), 1 wt % BSA, 25 mM EDTA, and 50% (v/v) glycerol and kept at 4 °C for 4 h. Then, FPs were suspended using vortex at 4 °C. The fecal proteins were extracted by centrifuging the mixture for 15 min at 16,000g at 4 °C. The supernatants were collected and stored at −20 °C until they are required. At day 35, intestinal segments of the jejunum and colon from immunized mice were collected and carefully weighed after removing feces and washing with cold PBS. A certain amount of 1× PBS was

https://dx.doi.org/10.1021/acsomega.0c01792
ACS Omega 2020, 5, 18185−18197

added to make 0.1 g/mL of the samples. Then, these samples were centrifuged at 16,000*g* for 20 min at 4 °C. The supernatants containing mucosal IgA were collected and stored at −80 °C until they were required.

The level of OVA-specific antibodies including total IgG, IgG1, and IgG2a and IgA was determined by ELISA. Briefly, OVA was diluted in 0.1 M sodium carbonate buffer (pH 9.5) to a final concentration of 1 μg/mL, and 100 μL of OVA per well was used to coat 96-well plates, followed by overnight incubation at 4 °C. After removing OVA solution, the plates were washed three times with washing buffer (1× PBS containing 0.1% Tween-20) and blocked with PBS-T containing 3% BSA for 2 h at room temperature with gentle shaking. After three washes, to each well was added 100 μL of diluted serum (1:25 to 1:3200) or diluted intestinal samples (1:5 to 1:1600) from the immunized mice, and the mixture was incubated for 2 h at 37 °C. After washing, 1× PBS containing 0.05% Tween-20 and 100 μL of horseradish peroxidase (HRP)-conjugated goat anti-mouse IgG, IgG1, or IgG2a antibody or goat anti-mouse IgA antibody (1:2000) was added to the plates. After 2 h incubation, the plates were washed four times with washing buffer. One hundred microliters of enzyme substrate 3,3′,5,5′-tetramethybenzidine (TMB) solution was added to each well and incubated for 30 min at room temperature. Then, 100 μL of 1 M H_2SO_4 was added to each well to stop the chromogenic reaction. The optical density (OD) of the samples was measured at 450 nm using a Tecan Infinite M200 Pro Plate Reader. The anti-OVA IgG or IgA antibody titers were defined as the dilutions ratio of the sample when the OD_{450nm} value was equal to 2.5× the background OD_{450nm} value.

Statistical Analysis. All the experiments were performed in triplicate, and data were analyzed by one-way and two-way ANOVA with Bonferroni post-tests using GraphPad Prism 7.0 software. A p value of <0.05 was considered statistically significant. *p < 0.05; **p < 0.01; ***p < 0.001; ****p < 0.0001.

RESULTS AND DISCUSSION

Physicochemical Properties of CaP-Based NPs. In this work, the CaP NPs were prepared via a water-in-oil microemulsion method based on our previous study[20] and the synthesis route is illustrated in Figure S1. Various CaP NPs were prepared by adjusting the molar ratio of Ca to P from 10 to 100. The surface charge of the CaP NPs changed from +4.8 to +8.3 mV with increasing Ca/P molar ratio (Table S1), reflecting the increasing excess of Ca^{2+}. The XRD pattern of the CaP NPs shown in Figure 1 and Figure S2 exhibits diffraction peaks at 25.1° and 31.9°, corresponding to the (002) and (012) diffractions of the apatite phase $Ca_{10}(PO_4)_6(OH)_2$, as well as peaks at 9.2° and 16.3° corresponding to the (020) and (112) diffractions of the β-tricalcium phosphate phase. These XRD results indicate that the CaP NPs consists of a biphasic mineral of hydroxyapatite and β-tricalcium phosphate.[34] No clear trend with preparation conditions in the relative ratio of the two phases was apparent.

The current study focused on CaP NPs prepared from a Ca/P ratio of 50 (based on BSA-FITC encapsulation optimization, which is detailed below). As shown in Figure 1A (i and v), the CaP NPs prepared with the Ca/P molar ratio of 50 had a spherical morphology with an average particle size of 14 nm. BSA-FITC was encapsulated into the CaP NPs during particle fabrication. When BSA-FITC was incorporated into CaP NPs, CaP@BSA-FITC NPs retained their spherical morphology, but their size increased to 22 nm as determined from TEM (Figure 1A, ii and iv). The zeta potential changed from positive (+6.4 mV) for the CaP NPs to negative (−9.6 mV) for CaP@BSA-FITC NPs, which can be attributed to incorporation of the low-pI protein BSA-FITC. The TEM image of CaP@BSA-FITC NPs using a negative stain (Figure S3) shows that BSA-FITC was loaded both inside and outside the CaP NPs. The outer layer of BSA on the CaP surface was 3−6 nm in thickness, which is equivalent to a BSA-FITC monolayer.[35]

The CaP@BSA-FITC NPs were subsequently coated with chitosan and alginate. Throughout the process of BSA encapsulation and coating with the polyelectrolytes chitosan and alginate, the XRD peaks of all samples (Figure 1B) were very similar, indicating that the biphasic mineral is maintained. The TEM images in Figure 1A (iii and iv) show that the CaP-Chi@BSA-FITC and CaP-Chi-Alg@BSA-FITC NPs maintained spherical morphology and that the size increased from 22 to 26 nm upon coating with chitosan and subsequently to 35 nm after coating with alginate. This indicates that the thickness of the dry chitosan coat in vacuum is 2 nm, while that of alginate is 4−5 nm. Coating of the CaP@BSA-FITC NPs with chitosan causes charge reversal with a change in zeta potential from −9.6 to +8.5 mV for CaP-Chi@BSA-FITC NPs when dispersed in DI water (pH 6), in agreement with chitosan being positively charged at this pH (pK_a = 6.5,[36] zeta potential of +12 mV at pH 6). After alginate adsorption, charge reversal is observed again with the CaP-Chi-Alg@BSA-FITC NPs displaying a zeta potential of −5.5 mV (pH 6), which is in agreement with the negative charge of alginate (pK_a = 3.5−3.7,[37] zeta potential of −32 mV at pH 6).

The process of BSA-FITC encapsulation and coating with chitosan and alginate was evaluated using FT-IR spectroscopy, as shown in Figure 1C. The spectrum of the CaP NPs featured characteristic bands at 1010−1020 (ν_3) and 566 (ν_4) cm^{-1}, corresponding to vibrational modes of the PO_4^{3-} unit of hydroxyapatite.[38] Due to the low encapsulation capacity of BSA-FITC in the CaP@BSA-FITC NPs (approximately 9%) and the highly hygroscopic nature of the particles, the new features observed as a strong band at 3400 cm^{-1} and a band at 1650 cm^{-1} are attributed to water absorbed on the NPs when exposed to ambient conditions after the drying process. The NPs with adsorbed polyelectrolytes appear to be less hygroscopic and the bands observed in the 3400 cm^{-1} region are attributed mainly to the H−O vibrational modes from the saccharides. Upon adsorption of chitosan, bands are observed at 1650 and 1545 cm^{-1} in the CaP-Chi@BSA-FITC NPs. These are in good agreement with those previously observed for chitosan in which a portion of the amine groups are protonated and can be assigned to amide I and antisymmetric $-NH_3^+$ deformation for the band at 1650 cm^{-1}, while the band at 1545 cm^{-1} is due to amide II and N−H bending vibration as well as the symmetric $-NH_3^+$ deformation.[29] This indicates that chitosan is interacting through attractive electrostatic forces with the BSA-FITC on the surface of the CaP@BSA-FITC NPs. In the CaP-Chi-Alg@BSA-FITC NPs, the band at 1650 cm^{-1} is broadened and a new band was observed at 1417 cm^{-1}, which can be attributed to the presence of the antisymmetric and symmetric COO^- stretching vibrations of alginate, respectively.[29] The lack of a vibrational mode at 1720 cm^{-1} indicates that alginate is in its deprotonated form and is thus interacting with the underlying chitosan layer through electrostatic attractive forces. Overall, the FTIR in conjunction

https://dx.doi.org/10.1021/acsomega.0c01792
ACS Omega 2020, 5, 18185−18197

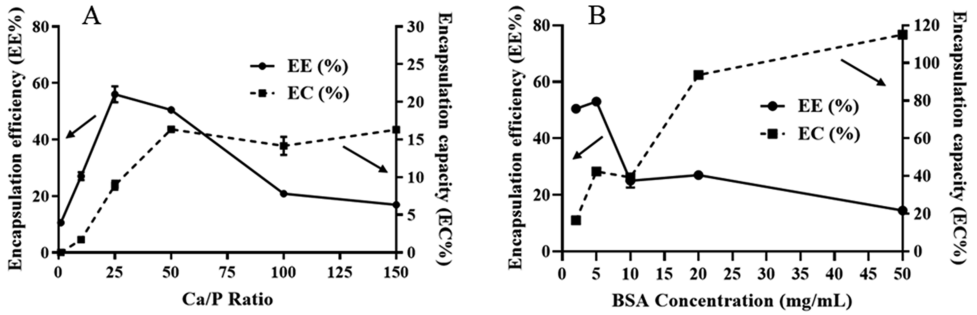

Figure 2. Encapsulation efficiency and capacity of BSA-FITC in CaP NPs at (A) different molar ratios of Ca/P (1, 10, 25, 50, 100, and 150) with a BSA-FITC concentration of 2 mg/mL and (B) different BSA-FITC concentrations (2, 5, 10, 20, and 50 mg/mL) with a Ca/P ratio of 50 (n = 3).

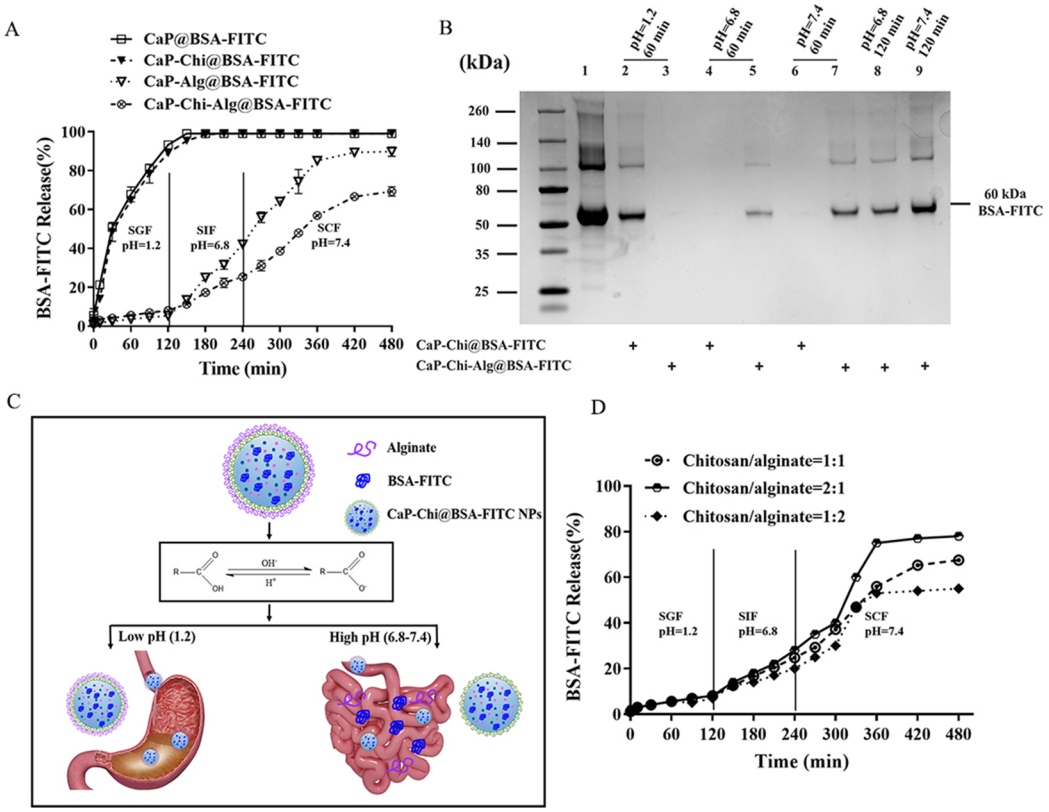

Figure 3. (A) BSA-FITC release from CaP-based NPs at different pH values including simulated gastric fluid (SGF, pH 1.2), simulated intestinal fluid (SIF, pH 6.8), and simulated colonic fluid (SCF, pH 7.4) (n = 3). (B) SDS-PAGE of BSA-FITC release from CaP-based nanocomposites (lane 1: native BSA-FITC only; lanes 2 and 3: CaP-Chi@BSA-FITC and CaP-Chi-Alg@BSA-FITC in SGF for 1 h, respectively; lanes 4 and 5: CaP-Chi@BSA-FITC and CaP-Chi-Alg@BSA-FITC in SIF for 1 h; lanes 6 and 7: CaP-Chi@BSA-FITC and CaP-Chi-Alg@BSA-FITC in SCF for 1 h; lane 8: BSA-FITC released from CaP-Chi-Alg@BSA-FITC in SIF for 2 h; lane 9: BSA-FITC released from CaP-Chi-Alg@BSA-FITC in SCF for 2 h). (C) Mechanism scheme of BSA-FITC release from CaP-Chi-Alg@BSA-FITC in simulated gastrointestinal fluid. (D) *In vitro* antigen release studies of CaP-Chi-Alg@BSA-FITC with the various ratio of chitosan to alginate in simulated gastric fluid (SGF), simulated intestinal fluid (SIF), and simulated colonic fluid (SCF).

with the zeta potential data provides evidence that the two polyelectrolytes have been successfully adsorbed onto the CaP@BSA-FITC NPs.

Encapsulation Efficiency and Capacity of Protein (BSA-FITC) in CaP NPs. BSA-FITC was used as an antigen model for OVA in part of this study based on their similar pI values of 4.8 and 4.5, respectively. The encapsulation efficiency and capacity of BSA-FITC in CaP NPs were optimized with regard to the molar ratio of Ca/P and the antigen concentration used during NP synthesis. As shown in Figure 2A, the encapsulation efficiency increased from 10.7 to 58.0% when increasing the Ca/P molar ratio from 1 to 25 (at 2 mg/mL of BSA-FITC). However, further increasing the Ca/P ratio to 50 does not have a significant effect, while increasing the Ca/P ratio to 100 and 150 resulted in a decrease in the encapsulation efficiency to 16.7%. This is a similar phenomenon to that reported in our previous work evaluating dsDNA loading in lipid-coated CaP NPs.[20] Both BSA and dsDNA have an overall negative charge at pH of 6.8, which is used in the NP synthesis. The low BSA-FITC encapsulation in CaP NPs at the lower Ca/P ratio of 1 is ascribed to the high concentration of PO_4^{3-} that may form dense solid CaP NPs and compete with BSA-FITC in interaction with Ca^{2+}. When increasing the Ca/P ratio to 25, CaP@BSA-FITC NPs can be simultaneously

https://dx.doi.org/10.1021/acsomega.0c01792
ACS Omega 2020, 5, 18185−18197

formed during the CaP crystal formation, owing to the affinity of Ca^{2+} ions to PO_4^{3-} in the CaP NPs and to $-COO^-$ in BSA-FITC. Thus, the enhancement of protein encapsulation efficiency may result from the cross-linking between BSA-FITC and superfluous Ca^{2+}.[36] However, further increasing the Ca/P ratio to 100 reduced the precipitation yield of CaP, resulting in the decrease in BSA-FITC encapsulation efficiency. These observations demonstrate that the BSA-FITC encapsulation efficiency in CaP NPs was critically affected by the molar ratio of Ca to P. Similarly, the encapsulation capacity of BSA-FITC in CaP@BSA-FITC increased from 0.01 to 16.2 mg/g with the Ca/P ratio increasing from 1 to 50 and remained unchanged to a Ca/P ratio of 150. Based on the encapsulation efficiency and capacity of BSA-FITC in CaP NPs, the optimized molar ratio of Ca/P for BSA loading was 50.

The effect of the BSA-FITC concentration on its encapsulation efficiency and capacity in the CaP NPs at the Ca/P ratio of 50 was further studied. As shown in Figure 2B, the encapsulation efficiency of BSA-FITC dramatically decreased with the increase in BSA-FITC concentration from 2 to 50 mg/mL. However, the encapsulation capacity of BSA-FITC in CaP@BSA-FITC NPs increased from 16.2 to 90.3 mg/g by increasing the BSA-FITC concentration from 2 to 20 mg/mL and increased further at the BSA-FITC concentration of 50 mg/mL. Based on both the encapsulation capacity and efficiency data, the maximal BSA loading capacity is 90 mg/g CaP NPs. The optimized synthetic condition for CaP@BSA is at the concentration of BSA-FITC of 20 mg/mL with a Ca/P ratio of 50. Subsequent experiments thus used these conditions for the preparation of CaP@protein NPs with a BSA-FITC loading of 90 mg/g CaP NP.

***In Vitro* Release of BSA-FITC in Simulated Gastrointestinal Fluid.** Simulated gastrointestinal fluids (pH adjusted solutions) were used to evaluate the capacity of the different CaP NPs to control the release of the antigen with the aim of improving the retention in the stomach fluid against premature release while optimizing release in the intestine. One additional sample was used in this study, a NP with a single coating of alginate, CaP-Alg@BSA-FITC (24 nm), to evaluate the effect of chitosan on drug release in the simulated intestinal fluid (SIF) and simulated colonic fluid (SCF) environments. As shown in Figure 3A, when immersing the particles in simulated gastric fluid (SGF, pH 1.2), 82 and 83% of BSA-FITC was released from CaP@BSA-FITC and CaP-Chi@BSA-FITC NPs, respectively, in the first 2 h. This can be attributed to the dissolution of the basic CaP minerals in the core of the NPs in the acidic conditions. In contrast, a much smaller fraction of BSA-FITC of 5 and 7% was released from the CaP-Alg@BSA-FITC and CaP-Chi-Alg@BSA-FITC NPs, respectively, under the same conditions, indicating that the alginate coating protects the dissolution of the CaP core and thereby significantly inhibits the release of BSA-FITC in the SGF. A similar observation has been made in previous studies using alginate coatings on NPs for vaccine delivery.[25,37] The excellent protection by alginate may be attributed to protonation of the majority of the carboxyl groups in alginate at this pH, which is two pH units below the pK_a value. This results in the formation of an alginic acid gel at the NP surface, as illustrated in Figure 3C. After 2 h incubation in SGF, the NPs were transferred to a solution with pH of 6.8 to simulate the NPs entering the intestinal environment. During the 2 h incubation in SIF, 40% of BSA-FITC was sustainably released from the CaP-Alg@BSA-FITC NPs, while only 20% was released from the CaP-Chi-Alg@BSA-FITC NPs. The release of BSA-FITC under these conditions can be ascribed to the deprotonation of the alginic acid layer and dissolution of alginate, especially when there is no underlying chitosan layer to interact with, e.g., in the CaP-Alg@BSA-FITC NP system. The slower release of the dual chitosan- and alginate-coated NPs illustrates that the chitosan layer is retained on the particle and provides a barrier for BSA-FITC diffusion from the particles. The fate of the alginate layer in the CaP-Chi-Alg@BSA-FITC NP system will be discussed further below. After 2 h incubation in SIF, the solution was adjusted to pH 7.4 to simulate the NPs entering the environment of the colon. Under these conditions, the release profile of BSA-FITC from the CaP-Alg@BSA-FITC and CaP-Chi-Alg@BSA-FITC NPs was similar over a 4 h period, resulting in a cumulative release of 85 and 60%, respectively. This result shows that co-coating of chitosan and alginate on the CaP surface significantly decreased the BSA-FITC release rate in the SIF.

To further examine the BSA-FITC release, SDS-PAGE was used to evaluate the relative amounts of BSA-FITC present in the simulated environments, comparing the CaP-Chi@BSA-FITC and CaP-Chi-Alg@BSA-FITC NP systems. In this study, the NPs were immersed in a single solution and the data are presented in Figure 3B where the black band at 60 kDa, lane 1, is due to the presence of BSA-FITC. This band was observed after incubation in SGF for 1 h for the CaP-Chi@BSA-FITC NPs (lane 2) but not for the CaP-Chi-Alg@BSA-FITC NPs (lane 3), in agreement with the absorbance measurements (Figure 3A), indicating the release of BSA-FITC only for the chitosan-coated NPs. Upon incubation of the NPs in a solution with pH of 6.8 or 7.4, no bands could be observed for the CaP-Chi@BSA-FITC NPs (lanes 4 and 6), indicating that the chitosan coating in these environments prevents diffusion of BSA-FITC from the NPs or, alternatively, that the BSA-FITC is released as a polyelectrolyte complex that is too large to move on the gel.[38] For the CaP-Chi-Alg@BSA-FITC NPs, the BSA-FITC band was observed in lanes 5 and 7, indicating the release of BSA-FITC in the pH 6.8 and 7.4 solutions after 1 h. A longer incubation time to 2 h results in larger amounts of BSA-FITC released (lanes 8 and 9) in these two solutions, indicating sustained release. Based on the relative intensity of the BSA-FITC band comparing pH 6.8 and 7.4 (lane 5 compared to 7 and lane 8 compared to 9), it would appear that the release is faster at pH 7.4. This could be related to the lower degree of protonation of chitosan at pH 7.4 compared to pH 6.8, resulting in greater dissociation of the alginate layer, thereby decreasing the diffusion barrier for BSA-FITC.

The effect of the mass ratio of chitosan to alginate (keeping the chitosan content constant) on the BSA-FITC release from the CaP-Chi-Alg@BSA-FITC was evaluated and the data are shown in Figure 3D. It was found that the BSA-FITC release rate remained the same in the SGF and in the SIF for the first 4 h, regardless of the ratio of chitosan to alginate. This demonstrates that even for the NP system with a lower amount of alginate (sample 2:1), there is sufficient alginate present to protect against BSA-FITC release in the SGF. After the particles were transferred to the SCF (pH 7.4), the release of BSA-FITC was observed to correlate with the amount of alginate added for the second coating. That is, the larger the amount of alginate, the slower the release. The similar release profile observed in SIF but a different profile in SCF indicates that the alginate layer, at least to some extent, is retained in the SIF but dissolved into solution in the SCF due to the reduced

https://dx.doi.org/10.1021/acsomega.0c01792
ACS Omega 2020, 5, 18185−18197

electrostatic attraction to the chitosan layer (one pH unit above the pK_a value), as also concluded from the SDS-PAGE data (Figure 3B).

The combined data indicate that the presence of an alginate layer prevents BSA-FITC release in the SGF, in which the chitosan layer is controlling the release in the SIF by providing a diffusion barrier and, to some extent, prevents the dissolution of alginate. Furthermore, in the SCF, the alginate layer dissociates from the NPs, the rate depending on the ratio of chitosan to alginate. Therefore, the dual coating system of chitosan and alginate is required to protect the CaP NPs in the acidic conditions and retained a large fraction of the antigen within the CaP NPs in the intestinal fluid followed by sustained release in the colon. Considering a continuous release of BSA-FITC in the SIF and SCF for the NPs prepared from the 1:1 mass ratio (representing a 15% molar excess of chitosan monomer units compared to alginate units), this is considered the optimal NP system.

Cellular Uptake and Cytotoxicity. It was discussed above that the key function of the alginate layer is to protect the CaP NPs and the BSA-FITC against dissolution and degradation, respectively, in the acidic environment of the gastric fluid. However, once it has fulfilled this role, it dissociates from the NP surface and, thus, the relevant NP systems to evaluate with regard to *in vitro* studies are CaP@BSA-FITC and CaP-Chi@BSA-FITC. The cytotoxicity of the CaP@BSA-FITC and CaP-Chi@BSA-FITC to Caco-2 and RAW264.7 cells was evaluated via an MTT assay at CaP concentrations of 50−400 μg/mL. As shown in Figure S4, the cell viability of the NPs in this concentration range was above 80% for both Caco-2 and RAW 264.7 cells after 48 h incubation, indicating that the NPs do not cause acute toxicity *in vitro* even at a concentration of 400 μg/mL, which is consistent with our previous report.[20]

Human epithelial colorectal cells (Caco-2) were selected to represent the enterocytes encountered by the NPs during oral administration. Using confocal laser scanning microscopy, the colocation of FITC (green fluorescence) and DAPI nucleus staining (blue fluorescence) was evaluated (Figure 4A). The cells treated with free BSA-FITC for 8 h had only a few green fluorescence areas, and these were observed in the perinuclear region of Caco-2 cytoplasm, as indicated by the arrow in the merged image. In comparison, a large number of green fluorescent areas were observed for cells incubated with CaP@BSA-FITC and CaP-Chi@BSA-FITC for 8 h and these areas were found to co-localize with the nucleus, indicating that BSA-FITC was efficiently delivered into the Caco-2 cells by the NPs. Flow cytometry (FACS) was used to quantify the mean fluorescence intensity from BSA-FITC associated with the Caco-2 cells after incubation with free BSA-FITC or the CaP@BSA-FITC and CaP-Chi@BSA-FITC NPs for 8 h. The data represented in Figure 4B,C reveal that the cellular uptake of BSA-FITC was both time- and dose-dependent (BSA-FITC concentration from 0.5 to 8.0 μg/mL; time, 1 to 24 h). The percentage of Caco-2 cells that were BSA-FITC-positive was significantly larger for the NP-treated cells compared to cells treated with free BSA-FITC and this was evident for all time points and all concentrations investigated. This is in agreement with the CLSM data described above. For cells incubated with CaP@BSA-FITC and CaP-Chi@BSA-FITC (1 μg/mL BSA-FITC), the percentage of cells that were BSA-FITC-positive increased significantly from 1 to 24 h. Increasing the BSA-FITC concentration to 4 μg/mL (Figure 4C) allows for

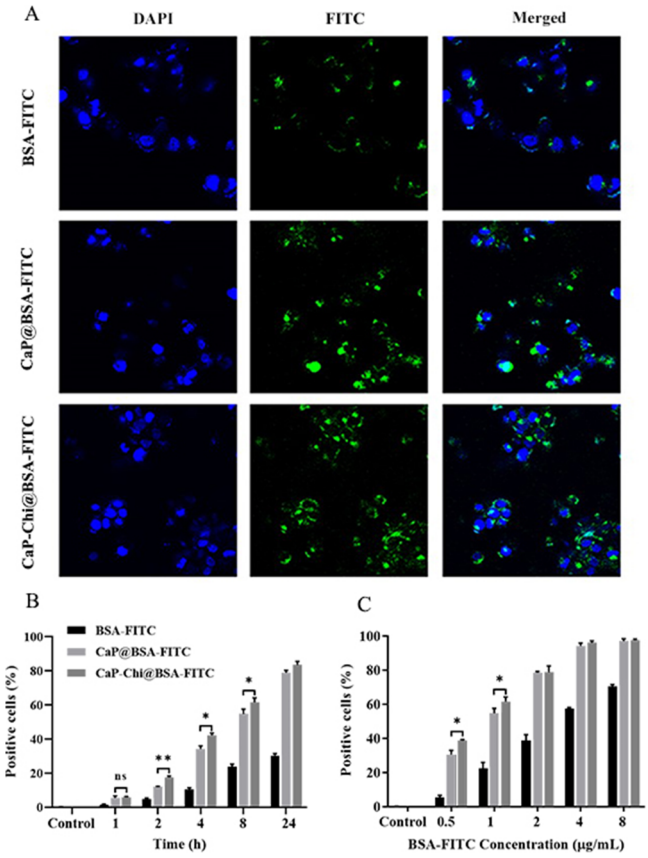

Figure 4. Cellular uptake efficiency of BSA-FITC, CaP@BSA-FITC, and CaP-Chi@BSA-FITC NPs in Caco-2 cells. (A) Fluorescence microscopy images of Caco-2 cells cultured with cargos for 8 h (1 μg/mL of BSA-FITC). (B) Effect of incubation time on the internalization of CaP@BSA-FITC and CaP-Chi@BSA-FITC NPs with BSA-FITC concentration of 1 μg/mL and (C) effect of dose on the internalization of CaP@BSA-FITC and CaP-Chi@BSA-FITC NPs with the incubation time of 8 h. Data represent mean ± SD. *$p < 0.05$ vs CaP NPs. **$p < 0.01$.

enhanced uptake compared to lower concentrations; however, further enhancement to 8 μg/mL shows no difference for either of the two NP systems. This trend indicates that the cellular uptake of BSA-FITC by the CaP-based NPs reached an uptake saturation after BSA-FITC is increased to 4 μg/mL. Notably, the cells incubated with the CaP-Chi@BSA-FITC NPs exert higher uptake in comparison with cells incubated with the CaP@BSA-FITC NPs for a number of time points and BSA-FITC concentrations ($p < 0.01$). For example, the chitosan coating resulted in significant enhancement of cellular uptake of BSA-FITC to Caco-2 cells at the 8 h time point compared to the uncoated NPs. A similar effect of the mucoadhesive polymer chitosan was reported by Ji et al. who observed enhanced internalization of FITC-labeled insulin when applying a chitosan coating.[39] This can be attributed to the strong binding affinity of the positively charged chitosan to the lectin-like receptors on the cell membrane.[25]

Cellular uptake of BSA-FITC was evaluated in the mouse macrophage cell line RAW 264.7 to determine the ability of CaP-based NPs to enhance antigen internalization in antigen-presenting cells. The cellular uptake by the RAW 264.7 cells presented time and concentration dependence (0.5 to 8 h, 0.25 to 4 μg/mL, Figure 5), similar to that observed in Caco-2 cells. The CLSM data in Figure 5A demonstrate larger areas of green

https://dx.doi.org/10.1021/acsomega.0c01792
ACS Omega 2020, 5, 18185−18197

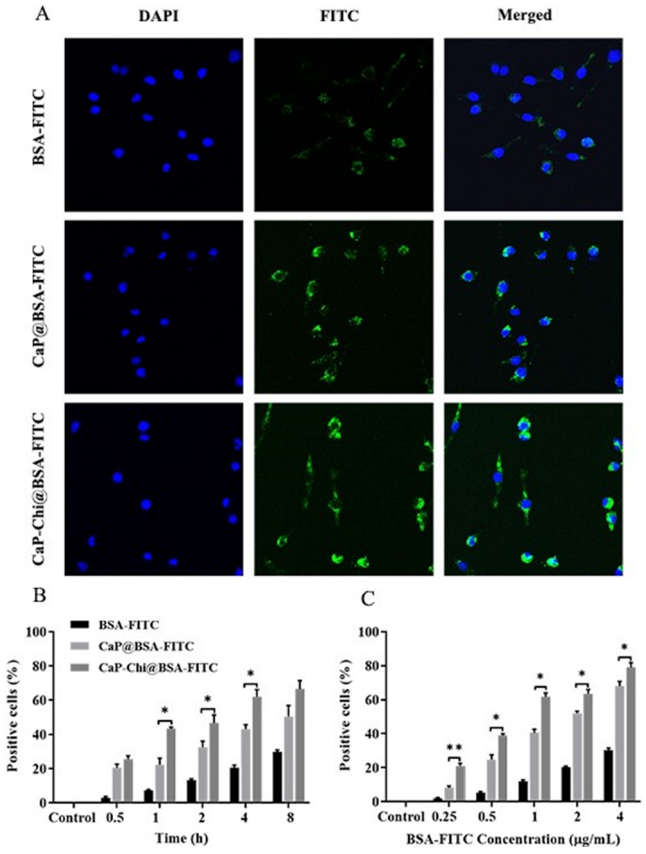

Figure 5. Cellular uptake efficiency of BSA-FITC, CaP@BSA-FITC, and CaP-Chi@BSA-FITC NPs in macrophage cells. (A) Fluorescence microscopy images of macrophage cells cultured with cargos for 4 h (1 μg/mL BSA-FITC). (B) Effect of incubation time on the internalization of CaP@BSA-FITC and CaP-Chi@BSA-FITC NPs with the BSA-FITC concentration of 1 μg/mL and (C) effect of dose on the internalization of CaP@BSA-FITC and CaP-Chi@BSA-FITC NPs with the incubation time of 4 h. Data represent mean ± SD. *p < 0.05 vs CaP NPs. **p < 0.01.

fluorescence signal from FITC for the cells exposed to the NP systems for 4 hours compared to cells exposed to BSA-FITC alone. This green fluorescence signal is co-located with the blue fluorescence signal from the DAPI nucleus stain. The FACS data presented in Figure 5B,C confirm that the cellular uptake of BSA-FITC is significantly larger when exposing the cells to the NP systems. Furthermore, it is evident from this result that the CaP-Chi@BSA-FITC-treated cells showed a higher positive cell percentage than those treated with CaP@BSA-FITC. Thus, this result indicates that the chitosan coating facilitated the BSA-FITC uptake by macrophages. This enhanced protein uptake is attributed to the positive charge of the CaP-Chi@BSA-FITC NPs as well as binding of chitosan to the mannose receptor on the macrophage surface. Macrophages and immature dendritic cells display high expression of the mannose receptor on the cell membrane and these mannose receptors have C-type carbohydrate recognition domains, which can recognize sugar ligands. The D-glucosamine and *N*-acetyl-D-glucosamine units of chitosan can bind strongly with the C-type carbohydrate recognition domains on the macrophage surface.[40] Thus, the importance of these findings is that the chitosan coating significantly facilitates the cellular uptake of BSA-FITC by macrophages and it can be inferred that a similar effect will apply to other antigen-presenting cells. This will cause effective promotion to B and T cells, where B cells will mature to produce immunoglobulins (also known as antibodies) and T cells become specifically cytotoxic, which show specific immune responses.[41]

Cell Surface Marker Expression. The expression of surface costimulatory molecules on antigen-presenting cells is of great relevance in further antigen presentation and the generation of an immune response. To investigate the stimulating effect of CaP and CaP-Chi NPs, OVA, a model antigen, was encapsulated into CaP and CaP-Chi NPs. The loading capacity of OVA in CaP is 90 mg/g, similar to BSA-FITC. Lipopolysaccharides (LPS), known to enhance the expression of cell surface markers by interacting with a specific membrane receptor, was used as the positive control and expression of cell surface molecules evaluated in mouse macrophage cell line RAW 264.7. The resulting data in Figure 6 show that the CaP NPs themselves significantly enhanced expression of the costimulatory molecules CD86, CD40, and MHC class II I-E/I-A compared to OVA at a concentration of 15 μg/mL. Further enhancement in stimulation was observed when OVA was encapsulated into CaP and CaP-Chi NPs (OVA concentration of 15 μg/mL) with significant enhanced expression of the costimulatory molecules CD80, CD86, CD40, and MHC class II I-E/I-A over nonstimulated cells. This demonstrates that the CaP NPs are a good adjuvant, concurring with a previous report.[42]

It is noteworthy that the CaP-Chi@OVA NPs induced a higher expression of CD80, CD40, and MHC class II molecule I-E/I-A compared to CaP@OVA NPs at the OVA concentration of 15 μg/mL. This is in agreement with the cellular uptake study in mouse macrophage cell line RAW 264.7 described above (Figure 5), where higher internalization of BSA-FITC was observed for the NP system with a chitosan coating. The enhanced expression of cell surface molecules can thus be ascribed to the better internalization of antigens by macrophages, which is aided by the targeting ability of chitosan to macrophages. As reported, chitosan microparticles can target the "glucosamine-like receptors" present on the surface of macrophage and due to its cationic nature, it can easily interact with cell membrane and facilitate endocytotic uptake.[43] This enhanced internalization may result in the endogenous signals, which are known to stimulate the immune responses.[44]

Oral Vaccination with CaP-Chi-Alg@OVA NPs. To evaluate the oral vaccination efficacy of antigens delivered by the CaP-Chi-Alg NPs, we investigated the *in vivo* mucosal antibody responses in a mouse model. Oral administration of PBS, OVA, and CaP-Chi-Alg@OVA was done by priming every second day, three times, in the first week, followed by a boost immunization at days 14 and 21 (Scheme 1). OVA (200 μg) was orally administered each time and a total of 1000 μg of OVA had been administered after 21 days. Figure S5 shows that the CaP-Chi-Alg NPs did not cause animal weight loss 35 days after oral vaccination, indicating good biocompatibility of the NP system. Production of a systemic anti-OVA antibody response was evaluated using serum analyzed at days 14 and 35. As shown in Figure 7A–F, the specific IgG level induced by the CaP-Chi-Alg@OVA NPs was higher at day 14, while the specific IgG, IgG1, and IgG2a levels were all significantly higher than OVA (and PBS) at day 35. The lack of enhanced levels of IgG1 and IgG2a antibodies generated by OVA and CaP-Chi-Alg@OVA NPs in the mouse model at day 14

https://dx.doi.org/10.1021/acsomega.0c01792
ACS Omega 2020, 5, 18185−18197

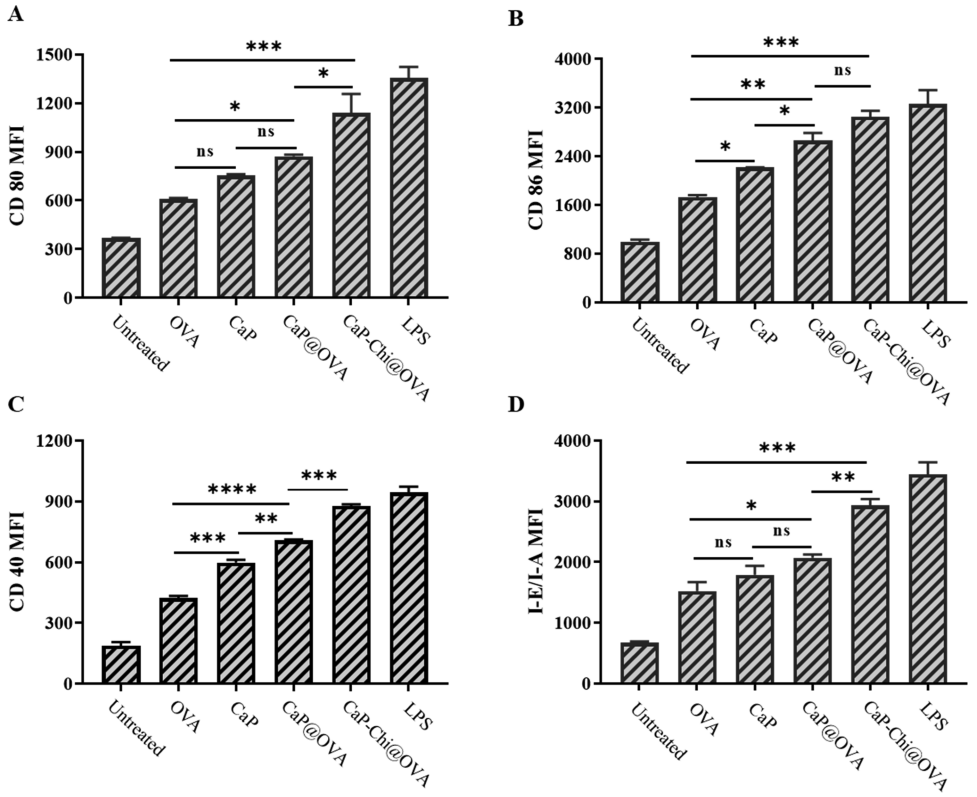

Figure 6. Expression of costimulatory molecules on the surface of macrophage (RAW 264.7) cells was studied by flow cytometry after incubation of cells with OVA, CaP, CaP@OVA, and CaP-Chi@OVA with an OVA concentration of 15 μg/mL for 24 h. Mean fluorescence intensity (MFI) expression of RAW 264.7 macrophage cell surface markers: (A) CD80, (B) CD86, (C) CD40, and (D) MHC II. Data represent mean ± SD. *p < 0.05, **p < 0.01, ***p < 0.001 from the nontreated macrophages.

Scheme 1. Oral Immunization Schedule[a]

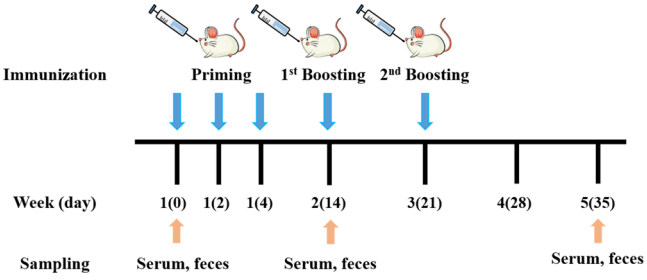

[a]Each group of mice was administrated five doses of the antigens, and serum and feces samples were collected as illustrated in the scheme.

(Figure 7D,F) indicates that stimulation of a specific IgG1 and IgG2a immune response requires a vaccine boosting and longer time for activation. The levels of IgG, IgG1, and IgG2a at day 35 indicate that OVA delivered by the CaP-Chi-Alg NPs produced a stronger antibody immune response than OVA itself and both have enhanced levels compared to PBS. So, while OVA itself is effective at this time point, a much stronger antibody immune response is observed when using the NP delivery system. Hannah et al. reported a chitosan-based OVA antigen oral delivery system, after four times administration and 35 day immunization, CS-encapsulated OVA, to induce 2-fold mucosal (IgA) immune response compared with the OVA group, while immunization with CS-OVA failed to increase the anti-OVA IgG response.[45] By comparison, based on our *in vitro* studies using BSA-FITC as a model (Figures 3−5), we can attribute the enhanced immune response observed for the NP system to the prevention of OVA degradation in the acidic conditions of the gastric fluid due to protection by the alginate coating and facilitated cellular uptake of OVA by the intestine cells aided by the chitosan coating.

The immunoglobulin-A (IgA) antibodies serve as the first-line defense in the gastrointestinal environment and prevent opportunistic infections. Production of a specific IgA anti-OVA immune response in the gut mucosa was measured using fecal extracts collected from the intestine of vaccinated mice and the results are shown in Figure 7G,H. Administration of OVA alone resulted in significantly higher levels of fecal IgA antibody at day 35 only, while significantly higher levels were detected in fecal extracts of mice vaccinated with CaP-Chi-Alg@OVA NPs (1000 μg of OVA) at both time points. The use of the NP system induced approximately 2-fold and 2.4-fold higher IgA levels (Figure 7G,H) at days 14 and 35, respectively, compared to OVA. The IgA immune response induced via the NPs dramatically increased with vaccination time, indicating that the CaP-Chi-Alg NPs were effective nanocarriers protecting the OVA antigen in the gastrointestinal tract and enhancing the OVA absorption in the small intestine. In a study by Snook et al., fiber-coated $CaCO_3$ microparticles were used for oral delivery of OVA to mice. With 1440 μg of OVA administrated, the microparticles-OVA group showed only moderate enhancement in IgA expression at day 35.[7] The higher IgA level induced by our delivery system with lower OVA dosage (1000 μg vs 1440 μg) possibly relates to the nanometric size of the CaP particles, the protective effect of alginate, and the mucosal penetrating property of chitosan. Based on these findings, we can conclude that CaP-Chi-Alg@

https://dx.doi.org/10.1021/acsomega.0c01792
ACS Omega 2020, 5, 18185−18197

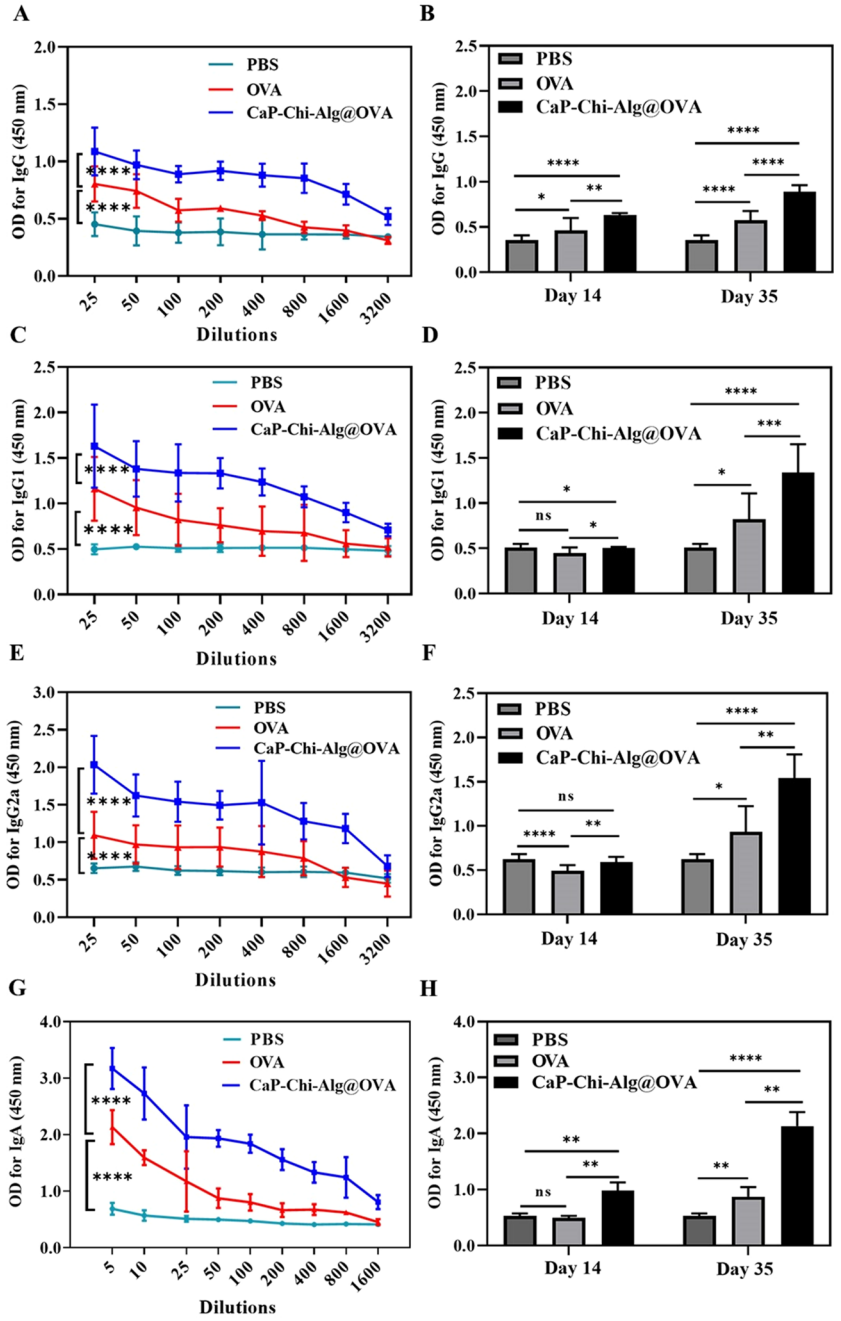

Figure 7. CaP-Chi-Alg@OVA induce immune responses to OVA. Dilution-dependent (A) anti-OVA IgG, (C) IgG1, and (E) IgG2a titer profiles of mice in sera collected at 35 days after immunization of female C57BL/6J mice (n = 6) with OVA adsorbed to CaP-Chi-Alg NPs or PBS; serum samples were analyzed at a dilution from 1:25 to 1:3200. (B) Anti-OVA IgG, (D) IgG1, and (F) IgG2a levels induced by CaP-Chi-Alg@OVA, PBS/OVA, and PBS at days 14 and 35 examined at a serum dilution of 1:100. (G) Dilution-dependent anti-OVA IgA titer profiles of mice in mice feces collected at 35 days (n = 6) after immunization of OVA adsorbed to CaP-Chi-Alg NPs or PBS; fecal samples were analyzed at a dilution from 1:5 to 1:1600. (H) Specific anti-OVA IgA secretion from fecal pellets at day 14 and intestinal mucosa at day 35 at a dilution of 1:50. Data are expressed as mean ± S.E.M. (n = 6). Statistically significant *p < 0.05; **p < 0.01; ***p < 0.001; ****p < 0.0001.

OVA NPs are effective at inducing strong mucosal antibody responses when administered orally.

CONCLUSIONS

We have demonstrated that chitosan- and alginate-coated CaP NPs have a great potential as an oral vaccine delivery vector. CaP-Chi-Alg NPs can efficiently encapsulate protein antigens into the CaP core with a particle size smaller than 50 nm. The alginate coating protects the antigens from degradation in the acidic gastric environment, while the chitosan coating affords sustained release of the antigen at pH 6.8 and 7.4 with the ability of adjusting the rate of release by manipulating the ratio of chitosan to alginate. Chitosan-coated CaP NPs enhance the internalization of protein antigens by Caco-2 cells and macrophages (antigen-presenting cells). *In vivo* oral vaccination tests demonstrated that OVA antigen delivered by CaP-Chi-Alg NPs significantly induced strong mucosal immune responses compared with OVA antigen itself. Therefore, chitosan- and alginate-coated calcium phosphate NPs is a promising carrier for oral delivery of protein antigens through

https://dx.doi.org/10.1021/acsomega.0c01792
ACS Omega 2020, 5, 18185−18197

the small intestine to elicit immune responses. Optimization of the polymer coating of this delivery system may enhance the immune response.

■ ASSOCIATED CONTENT

Supporting Information

The Supporting Information is available free of charge at https://pubs.acs.org/doi/10.1021/acsomega.0c01792.

Synthesis route of polymer-coated CaP; XRD characterization of CaP with different ratios of Ca and P; TEM images of negatively strained CaP@BSA-FITC; MTT assay analysis of polymer-uncoated and polymer-coated CaP NPs; animal weight during the oral vaccination process; surface charge of CaP NPs prepared at different Ca/P ratios (PDF)

■ AUTHOR INFORMATION

Corresponding Authors

Li Li − *Australian Institute for Bioengineering and Nanotechnology, The University of Queensland, Brisbane, QLD 4072, Australia;* orcid.org/0000-0001-6545-858X; Email: l.li2@uq.edu.au

Zhi Ping Xu − *Australian Institute for Bioengineering and Nanotechnology, The University of Queensland, Brisbane, QLD 4072, Australia;* orcid.org/0000-0001-6070-5035; Email: gordonxu@uq.edu.au

Authors

Pei Cao − *Australian Institute for Bioengineering and Nanotechnology, The University of Queensland, Brisbane, QLD 4072, Australia*

Felicity Y. Han − *Australian Institute for Bioengineering and Nanotechnology and School of Biomedical Sciences, Faculty of Medicine, The University of Queensland, Brisbane, QLD 4072, Australia*

Lisbeth Grøndahl − *Australian Institute for Bioengineering and Nanotechnology and School of Chemistry and Molecular Biosciences, The University of Queensland, Brisbane, QLD 4072, Australia;* orcid.org/0000-0001-6012-9808

Complete contact information is available at: https://pubs.acs.org/10.1021/acsomega.0c01792

Notes

The authors declare no competing financial interest.

■ ACKNOWLEDGMENTS

The authors thank associate facilities and the technical assistance of the Australian Microscopy & Microanalysis Research Facility at the Centre for Microscopy and Microanalysis (CMM) and Australian National Fabrication Facility (QLD Node), The University of Queensland. The study was financially supported by Advance Queensland Research Fellowship, Chinese Scholarship Council (CSC), and Australian Research Council (ARC) Discovery Projects (DP170104643 and DP190103486).

■ REFERENCES

(1) Del Giudice, G. Vaccination strategies. *Vaccine* **2003**, *21*, S83−S88.

(2) Des Rieux, A.; Fievez, V.; Garinot, M.; Schneider, Y. J.; Préat, V. Nanoparticles as potential oral delivery systems of proteins and vaccines: a mechanistic approach. *J. Controlled Release* **2006**, *116*, 1−27.

(3) Muheem, A.; Shakeel, F.; Jahangir, M. A.; Anwar, M.; Mallick, N.; Jain, G. K.; Warsi, M. H.; Ahmad, F. J. A review on the strategies for oral delivery of proteins and peptides and their clinical perspectives. *Saudi Pharm. J.* **2016**, *24*, 413−428.

(4) Qi, J.; Zhuang, J.; Lv, Y.; Lu, Y.; Wu, W. Exploiting or overcoming the dome trap for enhanced oral immunization and drug delivery. *J. Controlled Release* **2018**, *275*, 92−106.

(5) Morishita, M.; Peppas, N. A. Is the oral route possible for peptide and protein drug delivery? *Drug Discovery Today* **2006**, *11*, 905−910.

(6) Davitt, C. J. H.; Lavelle, E. C. Delivery strategies to enhance oral vaccination against enteric infections. *Adv. Drug Delivery Rev.* **2015**, *91*, 52−69.

(7) Snook, J. D.; Chesson, C. B.; Peniche, A. G.; Dann, S. M.; Paulucci, A.; Pinchuk, I. V.; Rudra, J. S. Peptide nanofiber−CaCO3composite microparticles as adjuvant-free oral vaccine delivery vehicles. *J. Mater. Chem. B* **2016**, *4*, 1640−1649.

(8) Kammona, O.; Bourganis, V.; Karamanidou, T.; Kiparissides, C. Recent developments in nanocarrier-aided mucosal vaccination. *Nanomedicine* **2017**, *12*, 1057−1074.

(9) Vela Ramirez, J. E.; Sharpe, L. A.; Peppas, N. A. Current state and challenges in developing oral vaccines. *Adv. Drug Delivery Rev.* **2017**, 116.

(10) Truong-Le, V.; Lovalenti, P. M.; Abdul-Fattah, A. M. Stabilization challenges and formulation strategies associated with oral biologic drug delivery systems. *Adv. Drug Delivery Rev.* **2015**, *93*, 95−108.

(11) Yun, Y.; Cho, Y. W.; Park, K. Nanoparticles for oral delivery: targeted nanoparticles with peptidic ligands for oral protein delivery. *Adv. Drug Delivery Rev.* **2013**, *65*, 822−832.

(12) Epple, M.; Ganesan, K.; Heumann, R.; Klesing, J.; Kovtun, A.; Neumann, S.; Sokolova, V. Application of calcium phosphatenanoparticles in biomedicine. *J. Mater. Chem.* **2010**, *20*, 18−23.

(13) Mueller, B.; Zacharias, M.; Rezwan, K. Bovine Serum Albumin and Lysozyme Adsorption on Calcium Phosphate Particles. *Adv. Eng. Mater.* **2010**, *12*, B53−B61.

(14) Ginebra, M. P.; Canal, C.; Espanol, M.; Pastorino, D.; Montufar, E. B. Calcium phosphate cements as drug delivery materials. *Adv. Drug Delivery Rev.* **2012**, *64*, 1090−1110.

(15) Masson, J. D.; Thibaudon, M.; Bélec, L.; Crépeaux, G. Calcium phosphate: a substitute for aluminum adjuvants? *Expert Rev. Vaccines* **2017**, *16*, 289−299.

(16) Temchura, V. V.; Kozlova, D.; Sokolova, V.; Überla, K.; Epple, M. Targeting and activation of antigen-specific B-cells by calcium phosphate nanoparticles loaded with protein antigen. *Biomaterials* **2014**, *35*, 6098−6105.

(17) Jani, P.; Halbert, G. W.; Langridge, J.; Florence, A. T. Nanoparticle uptake by the rat gastrointestinal mucosa: quantitation and particle size dependency. *J. Pharm. Pharmacol.* **1990**, *42*, 821−826.

(18) Lai, S. K.; Wang, Y.-Y.; Hanes, J. Mucus-penetrating nanoparticles for drug and gene delivery to mucosal tissues. *Adv. Drug Delivery Rev.* **2009**, *61*, 158−171.

(19) Wu, Y.; Gu, W.; Li, L.; Chen, C.; Xu, Z. P. Enhancing PD-1 Gene Silence in T Lymphocytes by Comparing the Delivery Performance of Two Inorganic Nanoparticle Platforms. *Nanomaterials* **2019**, *9*, 159.

(20) Tang, J.; Li, L.; Howard, C. B.; Mahler, S. M.; Huang, L.; Xu, Z. P. Preparation of optimized lipid-coated calcium phosphate nanoparticles for enhanced in vitro gene delivery to breast cancer cells. *J. Mater. Chem. B* **2015**, *3*, 6805−6812.

(21) Lin, Y.; Wang, X.; Huang, X.; Zhang, J.; Xia, N.; Zhao, Q. Calcium phosphate nanoparticles as a new generation vaccine adjuvant. *Expert Rev. Vaccines* **2017**, *16*, 895−906.

(22) Serag, M. F.; Kaji, N.; Gaillard, C.; Okamoto, Y.; Terasaka, K.; Jabasini, M.; Tokeshi, M.; Mizukami, H.; Bianco, A.; Baba, Y.

Trafficking and Subcellular Localization of Multiwalled Carbon Nanotubes in Plant Cells. *ACS Nano* **2011**, *5*, 493−499.
(23) Zhang, J.; Zhu, X.; Jin, Y.; Shan, W.; Huang, Y. Mechanism study of cellular uptake and tight junction opening mediated by goblet cell-specific trimethyl chitosan nanoparticles. *Mol. Pharmaceutics* **2014**, *11*, 1520−1532.
(24) Ribeiro, L. N. M.; Alcantara, A. C. S.; Darder, M.; Aranda, P.; Araújo-Moreira, F. M.; Ruiz-Hitzky, E. Pectin-coated chitosan-LDH bionanocomposite beads as potential systems for colon-targeted drug delivery. *Int. J. Pharm.* **2014**, *463*, 1−9.
(25) Yu, X.; Wen, T.; Cao, P.; Shan, L.; Li, L. Alginate-chitosan coated layered double hydroxide nanocomposites for enhanced oral vaccine delivery. *J. Colloid Interface Sci.* **2019**, *556*, 258−265.
(26) Xu, B.; Zhang, W.; Chen, Y.; Xu, Y.; Wang, B.; Zong, L. Eudragit(R) L100-coated mannosylated chitosan nanoparticles for oral protein vaccine delivery. *Int. J. Biol. Macromol.* **2018**, *113*, 534−542.
(27) Maity, S.; Mukhopadhyay, P.; Kundu, P. P.; Chakraborti, A. S. Alginate coated chitosan core-shell nanoparticles for efficient oral delivery of naringenin in diabetic animals-An in vitro and in vivo approach. *Carbohydr. Polym.* **2017**, *170*, 124−132.
(28) Bokkhim, H.; Bansal, N.; Grøndahl, L.; Bhandari, B. In-vitro digestion of different forms of bovine lactoferrin encapsulated in alginate micro-gel particles. *Food Hydrocolloids* **2016**, *52*, 231−242.
(29) Lawrie, G.; Keen, I.; Drew, B.; Chandler-Temple, A.; Rintoul, L.; Fredericks, P.; Grøndahl, L. Interactions between Alginate and Chitosan Biopolymers Characterized Using FTIR and XPS. *Biomacromolecules* **2007**, *8*, 2533−2541.
(30) Aston, R.; Wimalaratne, M.; Brock, A.; Lawrie, G.; Grøndahl, L. Interactions between Chitosan and Alginate Dialdehyde Biopolymers and Their Layer-by-Layer Assemblies. *Biomacromolecules* **2015**, *16*, 1807−1817.
(31) Pavlovic, M.; Rouster, P.; Szilagyi, I. Synthesis and formulation of functional bionanomaterials with superoxide dismutase activity. *Nanoscale* **2017**, *9*, 369−379.
(32) Sáringer, S.; Akula, R. A.; Szerlauth, A.; Szilagyi, I. Papain Adsorption on Latex Particles: Charging, Aggregation, and Enzymatic Activity. *J. Phys. Chem. B* **2019**, *123*, 9984−9991.
(33) Rouster, P.; Pavlovic, M.; Sáringer, S.; Szilagyi, I. Functionalized Titania Nanosheet Dispersions of Peroxidase Activity. *J. Phys. Chem. C* **2018**, *122*, 11455−11463.
(34) Piccirillo, C.; Silva, M. F.; Pullar, R. C.; Braga da Cruz, I.; Jorge, R.; Pintado, M. M. E.; Castro, P. M. L. Extraction and characterisation of apatite- and tricalcium phosphate-based materials from cod fish bones. *Mater. Sci. Eng., C* **2013**, *33*, 103−110.
(35) Cordeiro, A. L.; Rückel, M.; Bartels, F.; Maitz, M. F.; Renner, L. D.; Werner, C. Protein adsorption dynamics to polymer surfaces revisited-A multisystems approach. *Biointerphases* **2019**, *14*, No. 051005.
(36) Uskoković, V.; Uskoković, D. P. Nanosized hydroxyapatite and other calcium phosphates: chemistry of formation and application as drug and gene delivery agents. *J. Biomed. Mater. Res., Part B* **2011**, *96*, 152−191.
(37) Shrestha, N.; Araújo, F.; Shahbazi, M.-A.; Mäkilä, E.; Gomes, M. J.; Herranz-Blanco, B.; Lindgren, R.; Granroth, S.; Kukk, E.; Salonen, J.; Hirvonen, J.; Sarmento, B.; Santos, H. A. Thiolation and Cell-Penetrating Peptide Surface Functionalization of Porous Silicon Nanoparticles for Oral Delivery of Insulin. *Adv. Funct. Mater.* **2016**, *26*, 3405−3416.
(38) Bokkhim, H.; Bansal, N.; Grøndahl, L.; Bhandari, B. Interactions between different forms of bovine lactoferrin and sodium alginate affect the properties of their mixtures. *Food Hydrocolloids* **2015**, *48*, 38−46.
(39) Ji, N.; Hong, Y.; Gu, Z.; Cheng, L.; Li, Z.; Li, C. Chitosan coating of zein-carboxymethylated short-chain amylose nanocomposites improves oral bioavailability of insulin in vitro and in vivo. *J. Controlled Release* **2019**, *313*, 1−13.
(40) Han, Y.; Zhao, L.; Yu, Z.; Feng, J.; Yu, Q. Role of mannose receptor in oligochitosan-mediated stimulation of macrophage function. *Int. Immunopharmacol.* **2005**, *5*, 1533−1542.
(41) Lepenies, B.; Lee, J.; Sonkaria, S. Targeting C-type lectin receptors with multivalent carbohydrate ligands. *Adv. Drug Delivery Rev.* **2013**, *65*, 1271−1281.
(42) Sokolova, V.; Knuschke, T.; Kovtun, A.; Buer, J.; Epple, M.; Westendorf, A. M. The use of calcium phosphate nanoparticles encapsulating Toll-like receptor ligands and the antigen hemagglutinin to induce dendritic cell maturation and T cell activation. *Biomaterials* **2010**, *31*, 5627−5633.
(43) Ghaffarian, R.; Pérez-Herrero, E.; Oh, H.; Raghavan, S. R.; Muro, S. Chitosan-Alginate Microcapsules Provide Gastric Protection and Intestinal Release of ICAM-1-Targeting Nanocarriers, Enabling GI Targeting In Vivo. *Adv. Funct. Mater.* **2016**, *26*, 3382−3393.
(44) Seong, S. Y.; Matzinger, P. Hydrophobicity: an ancient damage-associated molecular pattern that initiates innate immune responses. *Nat. Rev. Immunol.* **2004**, *4*, 469−478.
(45) Cole, H.; Bryan, D.; Lancaster, L.; Mawas, F.; Vllasaliu, D. Chitosan nanoparticle antigen uptake in epithelial monolayers can predict mucosal but not systemic in vivo immune response by oral delivery. *Carbohydr. Polym.* **2018**, *190*, 248−254.

https://dx.doi.org/10.1021/acsomega.0c01792
ACS Omega 2020, 5, 18185−18197